RSC Advances

PAPER

View Article Online
View Journal | View Issue

Check for updates

Cite this: *RSC Adv.*, 2024, **14**, 9062

Effect of organoclay on the physical properties of colorless and transparent copoly(amide imide) nanocomposites

Changyub Na,[a] Lee Ku Kwac,[ab] Hong Gun Kim[ab] and Jin-Hae Chang *[b]

Received 17th December 2023
Accepted 12th March 2024

DOI: 10.1039/d3ra08605d

rsc.li/rsc-advances

Copoly(amic acid) was prepared using the diamine monomer *N*,*N*′-[2,2′-bis(trifluoromethyl)-4,4′-biphenylene]bis(4-aminobenzamide) (**TFAB**) and the anhydride monomers 4,4′-(hexafluoroisopropylidene)diphthalic anhydride (**6FDA**) and 4,4′-biphthalic anhydride (**BPA**). Thereafter, a colorless and transparent copoly(amide imide) (Co-CPAI) film was synthesized through various heat treatments. Co-CPAI hybrid films with a **TFAB** : **6FDA** : **BPA** molar ratio of 1 : 0.5 : 0.5 were subsequently fabricated using organically modified hectorite (STN) with various contents ranging from 0 to 7 wt% *via* the solution intercalation method. Finally, the thermomechanical properties, clay dispersion, and optical transmittance of the hybrid films were investigated. The results of wide-angle X-ray diffractometry and transmission electron microscopy demonstrated good dispersion at low clay loadings; however, clay agglomeration was observed above a certain critical STN content. At the critical STN content of 3 wt%, the clay was evenly distributed in the matrix with a nanoscale thickness of approximately 10 nm. Hybrid films containing 3 wt% STN showed excellent thermomechanical properties. Beyond this critical clay content, the physical properties of the films decreased because of the agglomeration of excess clay. Regardless of the clay content, however, the optical properties of the hybrid films remained constant, and their yellow indices, which ranged from 2 to 4, indicated excellent colorless transparency.

Open Access Article. Published on 18 March 2024. Downloaded on 6/4/2026 6:41:13 PM.
This article is licensed under a Creative Commons Attribution-NonCommercial 3.0 Unported Licence.

1. Introduction

Substrates considered suitable for flexible displays must have device characteristics that do not change even if their shape is changed or bent; they must also be resistant to humidity and insoluble in solvents.[1–3] The glass substrates that are widely used in existing displays are heavy, brittle, inflexible, and difficult to employ in roll-to-roll processes. Thus, the demand for substrates using polymer materials suitable for flexible displays is increasing. The polymer substrate currently used for such applications is a material that has attracted attention since the beginning of the development of flexible displays because it offers excellent insulation and flexibility and is easy to manufacture. However, compared with glass, its applications are limited by its poor thermal and chemical instability.

Aromatic polyimide (PI), a special engineering plastic with excellent heat resistance, chemical resistance, and insulation properties, is widely used in aerospace, military, and electronic materials. In recent years, increased research has been conducted to enable its application in flexible displays.[4,5] However, PI has poor processability because it is insoluble and infusible, and its use in transparent displays is limited by its unique dark brown color. Colorless and transparent PI (CPI) can be synthesized by preventing the intermolecular or intramolecular charge transfer complex (CTC) effect of the polymer chain.[6,7]

Several methods have been developed to overcome the CTC effect and synthesize CPI:[8–11] (1) reducing the linearity of the overall structure of the main chain by using a bent-shaped monomer, (2) disrupting the close packing between molecular chains by introducing substituents into the main chain, (3) introducing strong electron-withdrawing groups such as trifluoro methyl ($-CF_3$) or sulfone ($-SO_2-$) groups to inhibit the easy movement of π electrons in the aromatic ring, and (4) increasing the optical transparency of PI by using an alicyclic ring structure instead of an aromatic ring.

Compared with conventional PI, CPI has better optical properties but poorer thermal and mechanical properties because the use of a bent structure and introduction of high-electronegativity groups to its main chain, which are necessary to improve its optical properties, deteriorate its thermal and mechanical properties. Hence, the introduction of new monomer structures and compositions that can overcome these shortcomings and improve the physical properties of CPI while retaining its transparency should be considered.[12] One approach used to control polymer material properties involves the exploitation of the properties of various monomers through copolymerization. In general, the molecular regularity of

[a]*Graduate School of Carbon Convergence Engineering, Jeonju University, Jeonju 55069, Korea*

[b]*Institute of Carbon Technology, Jeonju University, Jeonju 55069, Korea. E-mail: changjinhae@hanmail.net*

© 2024 The Author(s). Published by the Royal Society of Chemistry

Open Access Article. Published on 18 March 2024. Downloaded on 6/4/2026 6:41:13 PM. This article is licensed under a Creative Commons Attribution-NonCommercial 3.0 Unported Licence.

copolyimide (Co-PI) is much lower than that of homopolyimide, which may lead to a decrease in interactions between polymer chains or molecules[13] and, in turn, changes in thermodynamic properties, transparency, solubility, *etc.* In addition, these properties of Co-PI can easily be controlled by appropriately adjusting the composition of the diamine and dianhydride monomers that make up the polymer.[14]

Research has been conducted to develop Co-PIs with improved thermomechanical properties despite their low transparency by using monomers with rigid structures. Many attempts to introduce functional groups such as esters, ethers, amides, and sulfones into the main chain to improve the low solubility and processability of these polymers owing to the aromatic structure and rigid main chain present in the PI structure have been reported.[15–17] Poly(amide imide) (PAI), which bears an amide group in the PI structure, exhibits excellent physical properties owing to the synergistic effect of amide and imide functional groups. Compared with other PIs, PAI exhibits higher thermomechanical properties, which are attributed to the hydrogen bonds between its amide chains and its excellent solubility in amide-based polar solvents. Given these advantages, PAI is used in a variety of applications, including adhesives, wire enamels, electronic devices, and extrusion and injection products.[18–20]

The thermomechanical properties of nanocomposites can be enhanced by uniformly dispersing nanosized fillers into the polymer matrix and maximizing the interfacial adhesion of these fillers to the polymer; such nanocomposites demonstrate better properties than blends or traditional composites. The available nanoscale fillers show superior organic–inorganic hybrid physical properties compared with traditional composite materials even when used in small amounts. Some common nanofillers include clay, carbon derivatives such as graphene or carbon nanotubes, layered double hydroxides, and polyhedral oligomeric silsesquioxane. Among these materials, clay is mainly used because it is easily procured, inexpensive, and convenient to process.[21,22]

Examples of smectite-based clays commonly used in nanocomposites include montmorillonite, saponite, bentonite, mica, and hectorite. Among these clays, hectorite can provide excellent thermal, tensile, and molecular barrier properties to the hybrid material because it is composed of laminated silicate sheets and has high swelling ability, which is essential for the efficient insertion of polymer chains.[23] The organic modification of pristine clays with long alkyl compounds is well known to facilitate the insertion of polymer chains into clay galleries. Hybrid studies have revealed that the dispersibility and compatibility of clay and polymer chains can be increased by using organically modified hectorite (STN) to facilitate the intercalation of polymer chains into the clay layers. These effects can further improve the physical properties of hybrid materials.[24,25]

During the synthesis of Co-CPI, the main chain must have a bent structure or an asymmetric substituent; thus, although the resultant material is both colorless and transparent, its thermal and mechanical properties are drastically reduced.[26,27] Therefore, a colorless and transparent copoly(amide imide) (Co-CPAI) was synthesized using a number of monomers with rigid structures to improve the thermomechanical properties of CPI while maintaining its transparency.[28–30]

In this study, we hypothesized that the introduction of an amide group to a monomer containing $-CF_3$ substituents during the synthesis of Co-CPAI will lead to improvements in thermomechanical properties owing to interchain hydrogen bonding within the Co-CPAI chains. To improve the physical properties of CPI while maintaining its optical transparency, we synthesized a new *N*,*N*′-[2,2′-bis(trifluoromethyl)-4,4′-biphenylene]bis(aminobenzamide) (**TFAB**) diamine monomer structure containing an amide group using the 2,2′-bis(trifluoromethyl) benzidine (TFB) portion of CPI. The monomers 4,4′-(hexafluoroisopropylidene)diphthalic anhydride (**6FDA**) with a highly electronegative trifluoromethyl ($-CF_3$) group and 4,4′-biphthalic anhydride (**BPA**) dianhydride with a rigid chain structure were used to improve the colorlessness and transparency of CPAI. Using these materials, we obtained a new Co-CPAI film with excellent optical properties by minimizing the decrease in thermal properties caused by improvements in colorlessness and transparency to the greatest extent possible.

The purposes of this study were to prepare Co-CPAI with a **TFAB** : **6FDA** : **BPA** molar ratio of 1.0 : 0.5 : 0.5 and to synthesize a hybrid film dispersed with various amounts of the organoclay STN (0–7 wt%) *via* the solution intercalation method. Subsequently, the thermomechanical properties, clay dispersibility, and optical transparency of the hybrid films were measured, and their physical properties were compared according to the content of organoclay.

2. Experimental

2.1 Materials

6FDA and **BPA** were purchased from TCI Co. (Tokyo, Japan). **TFAB** was synthesized directly in the laboratory.[31] All other reagents used in the synthesis procedures were purchased from TCI and Aldrich Chemical Co. (Yongin, Korea). *N*,*N*′-Dimethylacetamide (DMAc) was purified, moisture in the solvent was removed using a 4 Å molecular sieve, and general reagents were used without further purification. STN (Kunimine Ind. Co.) was organically modified so that the hectorite surface contained alkyl groups. The cation-exchange capacity of STN is 78 meq/100 g and its aspect ratio (length/width, *L*/*W*) is approximately 46.[32]

2.2 Synthesis of Co-CPAI and hybrid films

PI is generally synthesized from the poly(amic acid) (PAA) precursor state through various heat treatments. The conversion from PAA to PI mainly proceeds through a series of chemical reactions divided into two steps. This anhydride and diamine react to form PAA containing a carboxylic acid group (–COOH) and an amine group ($-NH_2$). These functional groups produce water as a by-product through various heat treatment processes, and the carboxylic acid and amine groups combine to form an imide bond. Through this reaction mechanism, PAA undergoes transformation into PI, resulting in the formation of

Open Access Article. Published on 18 March 2024. Downloaded on 6/4/2026 6:41:13 PM. This article is licensed under a Creative Commons Attribution-NonCommercial 3.0 Unported Licence.

a high-performance polymer with excellent thermal and mechanical stability.

The monomer structures and synthesis method for Co-CPAI are shown in Scheme 1. To obtain polyamic acid (PAA), we completely dissolved 20.24 g (3.62×10^{-2} mol) of **TFAB** in DMAc (200 mL) in a three-necked round flask at 0 °C under a N_2 atmosphere. Thereafter, 10.66 g (3.62×10^{-2} mol) of **BPA** and 14.49 g (3.26×10^{-2} mol) of **6FDA** were added to the **TFAB** solution and stirred first for 1 h at 0 °C and then for 18 h at room temperature for complete dissolution. The solid content of the obtained PAA was 18 wt%.

For chemical imidization, 18.50 g (1.81×10^{-1} mol) of acetic anhydride and 7.90 g (7.76×10^{-2} mol) of pyridine were added to the PAA solution at room temperature under a N_2 atmosphere for 1 h. After vigorous mixing at 80 °C for 2 h, the solution was added dropwise into 2 L of methanol to precipitate. The obtained PAA was dried in a vacuum oven at 100 °C for 12 h, redissolved in DMAc, and cast on a glass plate. After stabilization at 50 °C for 1 h under a N_2 atmosphere, thermal imidization was conducted by heat treatment first at 70 °C for 1 h and then at 100, 130, 160, 190, 220, or 250 °C for 30 min. Thereafter, the Co-CPAI film was removed by placing the glass plate in hot water. The thickness of the Co-CPAI hybrid films was maintained in the range of 33–35 μm to enable the reliable investigation of their physical properties and accurate comparison of their optical properties. The thickness of the films obtained by casting on a glass plate was measured using a micrometer, and the films were all colorless and transparent and showed bendable and rollable characteristics.

2.3 Characterization

The functional groups of the synthesized Co-CPAI films were confirmed using Fourier transform infrared (FT-IR; Spectrum Two, PerkinElmer, Llantrisant, UK) spectroscopy. ^{13}C magic angle spinning-nuclear magnetic resonance (^{13}C MAS-NMR; Bruker 400 MHz Advance II NMR Bruker, Berlin, Germany) was used. The Larmor frequency for ^{13}C MAS was $(\omega_0/2\pi)$ = 100.61 MHz and the MAS rate for ^{13}C was measured at 12 kHz to minimize the number of radiated side bands. The NMR peak was based on the signal corresponding to tetramethyl silane (TMS).

Wide-angle X-ray diffraction (XRD) analysis (X'Pert PRO-MRD, PANalytical, Amsterdam, Netherlands) was used to investigate the interlayer spacing (d) and overall dispersion state of the clay in the matrix. Cu-Kα was used as the target, the measurement speed was 2° min^{-1}, and measurements performed over the 2θ range of 2–15°. The simulated XRD pattern based on the data file is agrees well with the XRD experimental pattern. The XRD peaks observed in this diffractogram are confirmed using the JCPDS data base.[33,34] The dispersion state of the clays in the hybrid film was confirmed using field emission-scanning electron microscopy (FE-SEM; JSM-6500F, JEOL, Tokyo, Japan). To improve conductivity, the surface of the segmented film was sputtered with gold using an SPI sputter coater. Ultrathin specimens for transmission electron microscopy (TEM; JEM 2100, JEOL, Tokyo, Japan) were cured with epoxy and then heat-treated in a 70 °C oven for 24 h. Samples with a thickness of 90 nm were prepared using a microtome at an acceleration voltage of 120 kV under vacuum. The degree of dispersion of clay in the hybrid film could be measured through the scale bar shown in the TEM photographs.

A differential scanning calorimeter (DSC; S-650, SINCO) and thermogravimetric analyzer (TGA; Q500, TA) were used to analyze the thermal properties of the Co-PAI films under a N_2 atmosphere. The temperature increase rate was 20 °C min^{-1}. A thermal mechanical analyzer (TMA; TMA/SS100, SEIKO) was used to measure coefficients of thermal expansion (CTEs). The temperature was raised at a rate of 5 °C min^{-1} under a load of 0.1 N, and two cycles of heating were performed from 50 to 200 °C. All CTE values were determined from the second heating to obtain accurate results.

A universal testing machine (UTM; JP/AG-50KNX, SHIMADZU) was used to investigate the mechanical tensile properties of the films. The sample size was 5×50 mm^2, and the crosshead speed was 5 mm min^{-1}. Each sample was measured over 10 times, and the results were determined as the average within the error range.

Yellow index (YI) values were automatically determined using spectrophotometric measurements (CM-3600d, KONICA MINOLTA) at an observation angle of 10° with a CIE-D light source. The obtained values were then applied to the CIELAB color difference equation. The cut-off wavelength (λ_o) and light transmittance at 500 nm (500 nm^{trans}) were measured using a UV-vis spectrometer (UV-3600, SHIMADZU).

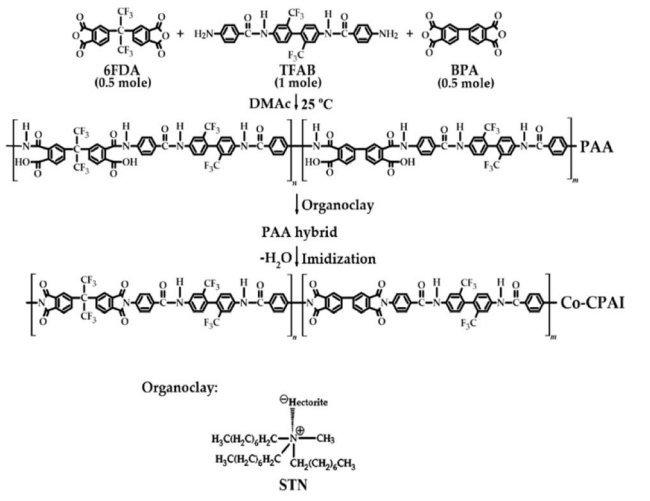

Scheme 1 Synthetic routes for Co-CPAI hybrid films.

3. Results and discussion

3.1 FT-IR and ^{13}C-NMR

The N–H stretching peak, which confirmed the presence of an amide group in the main chain, was observed at 3356 cm^{-1}, and the C=O asymmetric and symmetric carbonyl stretching peaks were observed at 1776 and 1710 cm^{-1}, respectively. The stretching peak of the imide bond at 1312 cm^{-1} confirmed the successful synthesis of Co-PAI, as shown in Fig. 1.[35]

© 2024 The Author(s). Published by the Royal Society of Chemistry

Open Access Article. Published on 18 March 2024. Downloaded on 6/4/2026 6:41:13 PM.
This article is licensed under a Creative Commons Attribution-NonCommercial 3.0 Unported Licence.

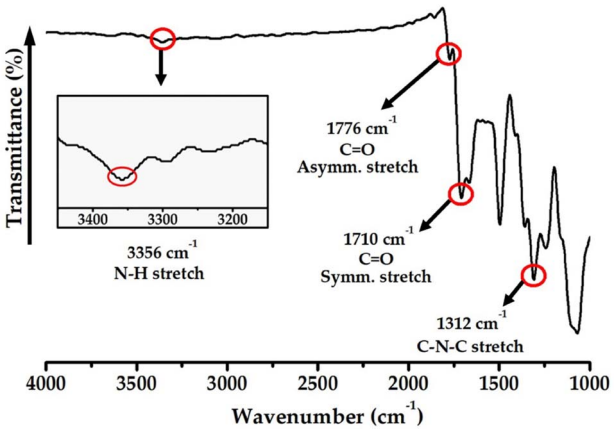

Fig. 1 FT-IR spectrum of Co-CPAI.

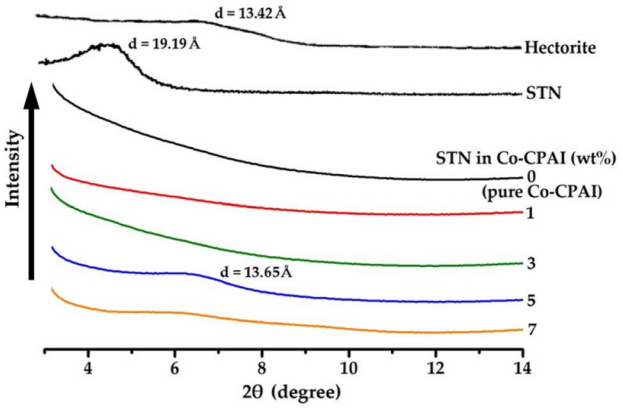

Fig. 3 XRD patterns of pristine clay, organoclay, and Co-CPAI hybrids with various STN contents.

The structural analysis of Co-CPAI was confirmed using ^{13}C CP/MAS NMR. The ^{13}C chemical shifts for each peak are shown in Fig. 2. Peaks a and c corresponding to the carbon atoms in dianhydride appeared at 68.18 ppm and 128.29 ppm, and carbons b, d, and e of benzene included in the dianhydrides were found at 121.34 ppm, 132.02 ppm, and 135.75 ppm. Additionally, carbons f and g in the diamine were observed at 141.45 ppm and 168.66 ppm. The sidebands of peak d (132.02 ppm) are marked with an asterisk (*), and the sidebands of 135.75 ppm (peak e) are marked with an open circle (o).[36] Ultimately, the structure of Co-CPAI was confirmed from the FT-IR and ^{13}C-NMR results described above.

3.2 Dispersibility using XRD

Fig. 3 shows the XRD patterns of pristine hectorite, STN, and Co-CPAI hybrid films dispersed with 0–7 wt% STN. Pristine hectorite showed a broad peak at $2\theta = 6.58°$ ($d = 13.42$ Å). Compared with that of pristine hectorite, the d of STN, which was prepared by organically modifying the hectorite surface with alkyl groups, increased to 19.19 Å ($2\theta = 4.60°$) because the alkyl groups widened the gap between clay layers.[12] This increase in d promotes the intercalation and dispersion of polymers into the clay layer, ultimately forming nanosized hybrid composites. As shown in Fig. 3, the characteristic peak of STN could not be observed in the hybrid films dispersed with up to 3 wt% STN. This result indicates that the clay was exfoliated from the polymer matrix when dispersed at up to 3 wt%. When the clay content exceeded 5 wt%, a weak diffraction peak appeared at $2\theta = 6.41°$ ($d = 13.77$ Å), probably because the clay was not evenly dispersed in the matrix and agglomerated when added at levels above the critical content.[37,38]

The peak positions of the hybrid films shifted toward higher 2θ values compared with those of STN, indicating that part of the clay collapsed within the polymer matrix. This result reveals that during the synthesis of CPAI by heat treatment in the PAA state in which the organoclay is dispersed, the decomposition of the organic components in STN caused by heating causes the clay layer to collapse and reduces d. Yano *et al.*[39] reported that organic molecules weakly bound to the clay surface were separated by heat treatment during the imidization of PAA to PI. The separation of organic materials that occurs owing to the heat treatment of the organoclay can further reduce d compared with that of STN.[40]

XRD data are very useful in determining the degree of dispersion or d of clay resulting from the insertion of polymers between clay layers in the hybrid films, but these results are one-dimensional and inaccurate for analyzing delaminated and exfoliated materials. Therefore, such data must be verified through electron microscopy to cross-check the results and observe the detailed intercalation or exfoliation of fillers in the nanoscale hybrid films.[41,42]

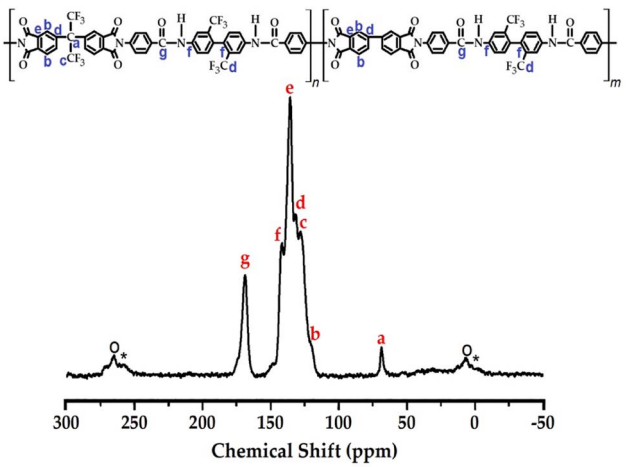

Fig. 2 ^{13}C-NMR chemical shift of Co-CPAI.

3.3 Morphology using electron microscopy

The results using electron microscopy complement the XRD results and provide a more detailed understanding of the dispersion state of the clay in the hybrid film. FE-SEM was used to compare the morphologies of neat Co-CPAI and Co-CPAI hybrid films with different clay contents, and TEM was used to observe the specific shape and orientation of the dispersed clay particles.

Open Access Article. Published on 18 March 2024. Downloaded on 6/4/2026 6:41:13 PM.
This article is licensed under a Creative Commons Attribution-NonCommercial 3.0 Unported Licence.

As can be seen from the SEM images, no morphology was observed on the fracture surface of the pure Co-CPAI film without clay (Fig. 4a), but a rough fracture surface was observed in the Co-CPAI hybrid film containing 3.0 and 5.0 wt% STN. This was observed (see Fig. 4b and c). As the STN content increased to 5 wt%, the morphology of the rough fracture surfaces gradually decreased in size. This change is because the clay dispersed in the matrix acts as a nucleating agent and small crystalline regions are formed around the clay particles.

TEM can accurately determine the degree of dispersion of the clay layers present in the hybrid films because it makes use of ultrafine sections to provide direct evidence of the formation of nanoscale composites. TEM micrographs of hybrid films with 3 and 5 wt% STN taken at different magnifications are shown in Fig. 5. The dark hair-like lines in the TEM images represent 1 nm-thick layers of clay. All TEM images showed that the clay was evenly dispersed within the polymer matrix to form an exfoliated nanocomposite; however, in some cases, the clay was agglomerated and lumps larger than several tens of nanometers were observed.

The hybrid film containing 3 wt% STN (Fig. 5a) showed an uneven dispersion of clay in the matrix, with a thickness of less than 10 nm. When the STN content was increased to 5 wt%, the overall dispersion was similar to that when 3 wt% STN was used, but some parts of the hybrid film showed aggregated clay with an average thickness of less than 20 nm (Fig. 5b). These findings are similar to the XRD results (Fig. 3). The dispersion of clay at levels above the critical content exerts negative effects on the thermomechanical properties and optical transparency of the hybrid film, as will be discussed in the succeeding sections.

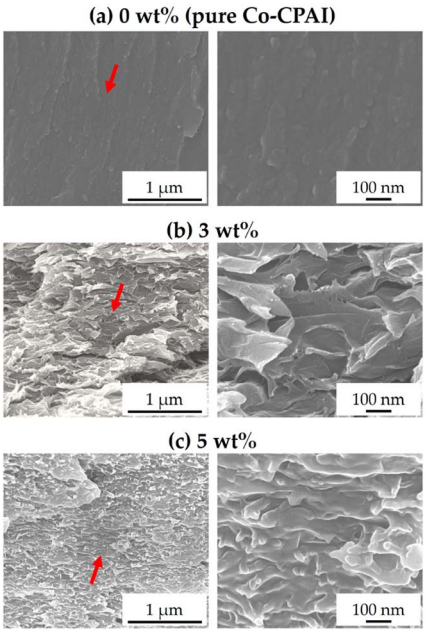

Fig. 4 SEM images of Co-CPAI hybrid films with various STN contents of (a) 0 wt% (pure Co-CPAI), (b) 3 wt%, and (c) 5 wt% at various magnifications.

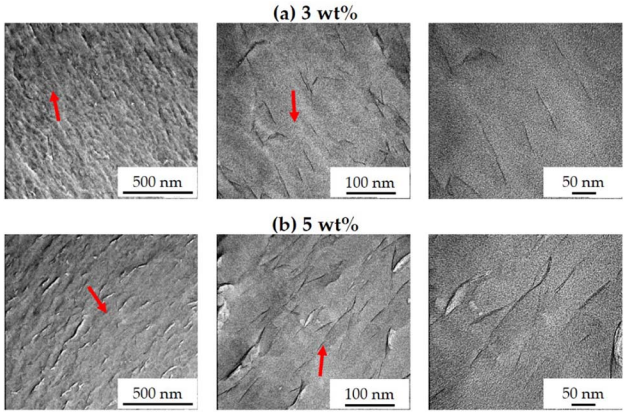

Fig. 5 TEM images of Co-CPAI hybrid films with various STN contents of (a) 3 wt% and (b) 5 wt% at various magnifications.

3.4 Thermal property

The thermal properties of hybrid films prepared with inorganic clay and organic polymers are known to increase owing to the high thermal stability of the clay. These effects can be used to optimize the thermal properties of composite materials. Since Co-CPAI is an amorphous polymer, its melt transition temperature cannot be measured by DSC; thus, in this study, thermal properties were explained in terms of the glass transition temperature (T_g). T_g is affected by the three-dimensional structure of the monomers that make up the polymer and the free volume owing to segmental motion, secondary bonds between main chains, the curing reaction, and types of functional groups and substituents. Especially in the case of hybrid materials, T_g is sensitive to the type and content of the dispersed filler.[43–45]

The thermal properties of Co-CPAI hybrids with various dispersed organoclay contents are summarized in Table 1. The T_g of pure Co-CPAI was 212 °C, while that of the hybrid film with 3 wt% STN was 233 °C. This increase in T_g is due to (1) the effect of the clay dispersed in the matrix on the free volume of the polymer chains and (2) the impediment of the movement of the polymer chains inserted within the clay galleries.[41,42] However, above a certain STN critical content, the T_g of the hybrid films tended to decrease. That is, when the STN content was increased from 3 to 7 wt%, T_g decreased from 233 to 213 °C, possibly because when the clay added to the hybrid film exceeds a certain critical concentration, it is not dispersed; instead, it aggregates, reducing T_g.[46,47] The aggregation of clay when the critical concentration is exceeded is supported by the XRD and TEM results (Fig. 3 and 5). Fig. 6 shows the DSC thermograms of Co-CPAI hybrids with different STN contents.

The change trend of the initial decomposition temperature (T_D^i), which indicates thermal stability, was similar to that of T_g. T_D^i showed a maximum value (452 °C) when the STN content was 3 wt%, as indicated in Table 1. Uniformly dispersed clay within the matrix polymer can enhance T_D^i by acting as a mass-transfer barrier for the volatile products generated during decomposition.[48–50] That is, polymer degradation may be delayed as the clay content increases in the hybrid film. This

© 2024 The Author(s). Published by the Royal Society of Chemistry

Open Access Article. Published on 18 March 2024. Downloaded on 6/4/2026 6:41:13 PM.
This article is licensed under a Creative Commons Attribution-NonCommercial 3.0 Unported Licence.

Table 1 Thermal properties of Co-CPAI hybrid films

STN in Co-CPAI (wt%)	T_g (°C)	$T_D^{i\,a}$ (°C)	$wt_R^{600\,b}$ (%)	CTE^c (ppm °C^{-1})
0 (pure Co-CPAI)	212	419	66	17.8
1	228	448	68	17.4
3	233	452	67	16.9
5	227	438	66	17.3
7	213	420	66	17.1

^{a} At a 2% initial weight-loss temperature. ^{b} Weight percent of residue at 600 °C. ^{c} Coefficient of thermal expansion for 2nd heating is 50–200 °C.

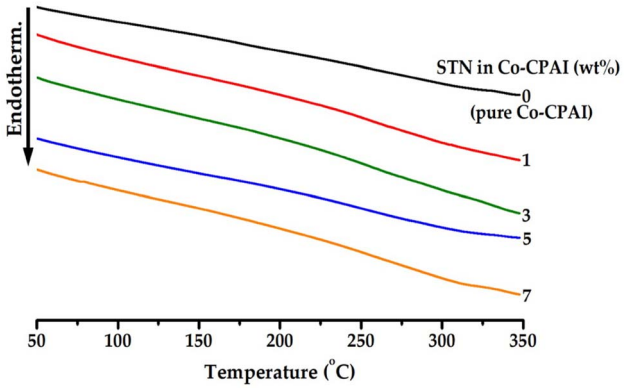

Fig. 6 DSC thermograms of Co-CPAI hybrids with various STN contents.

effect can be explained by the fact that the mobility of the polymer chains decreases as the nanosized clay particles become more evenly dispersed because inorganic clays are nondegradable materials with a very large surface area. The high dispersion of the nanoparticles in the polymer matrix presents an obstacle for the diffusion of free radicals, resulting in the retardation of the degradation of the nanocomposites. The increase in thermal stability of the hybrid films can also be attributed to the high thermal stability of the clay minerals. However, when 7 wt% STN was dispersed in the matrix, T_D^i rapidly decreased to 420 °C because the dispersion of clay contents beyond the critical content led to agglomeration. The finding that clay agglomerates above a certain critical concentration, leading to reductions in thermal stability, could be predicted from the T_g results. The residual weight (wt_R^{600}) upon heating up to 600 °C shows an almost-constant value of 66–68% for both pure Co-CPAI and the hybrid films, as indicated in Table 1. These results indicate that the organic substances in the organoclay STN do not have a significant effect on the thermal properties of the films. The TGA thermograms of Co-CPAI hybrid films with various STN contents are shown in Fig. 7.

Heat treatment of the pure polymer causes relaxation in the direction perpendicular to the polymer main chain. However, in the case of hybrid materials containing a hard and strong plate-shaped clay layer, relaxation becomes difficult owing to the thermal insulation of the clay. The addition of clay, which efficiently blocks heat transfer and has excellent thermal stability, can effectively suppress the lateral thermal expansion of the polymer during heat treatment.[51,52] The CTE values obtained in the second heating are summarized in Table 1, and the corresponding TMA thermograms of the films are shown in Fig. 8. The CTEs of pure Co-CPAI and the hybrid films were very low, at only 16.9–17.8 ppm °C^{-1}, regardless of the dispersed STN content.

Two factors are responsible for these very low CTE values. First, when the Co-CPAI hybrid film is heated, the Co-CPAI molecules arranged in the in-plane direction relax in the direction perpendicular to the original direction and eventually expand in the out-of-plane direction. However, the plate-shaped hectorites in the hybrid films are much harder than the CPAI molecules and are not easily deformed or expanded. As a result, the clay layer effectively prevents the thermal expansion of CPAI molecules in the out-of-plane direction. Second, the overall chain structure of Co-CPAI is mainly composed of benzene, which has excellent heat resistance, and an amide functional group that is capable of intramolecular hydrogen bonding.

3.5 Mechanical tensile property

Table 2 lists the mechanical properties (ultimate strength, initial modulus, and elongation at break (EB)) of Co-CPAI hybrid films with various STN contents. The ultimate strength and initial modulus of the pure Co-CPAI film were 87 MPa and 3.32 GPa, respectively, and increased to 122 MPa (40% higher) and 5.15 GPa (55% higher), respectively, when 3 wt% STN was dispersed in the films. The mechanical properties of the hybrid films are significantly influenced by the degree of dispersion

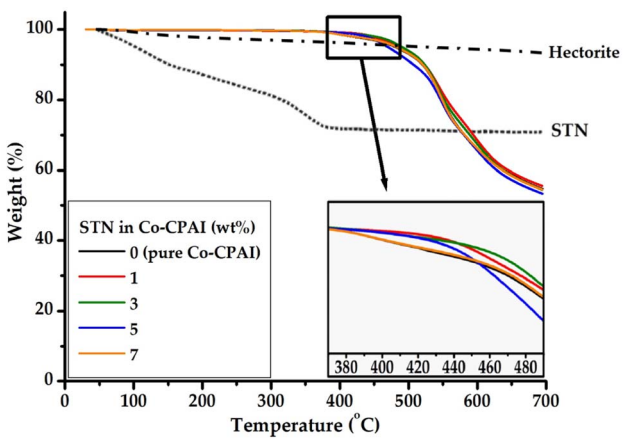

Fig. 7 TGA thermograms of pristine hectorite, STN, and Co-CPAI hybrids with various STN contents.

Open Access Article. Published on 18 March 2024. Downloaded on 6/4/2026 6:41:13 PM.
This article is licensed under a Creative Commons Attribution-NonCommercial 3.0 Unported Licence.

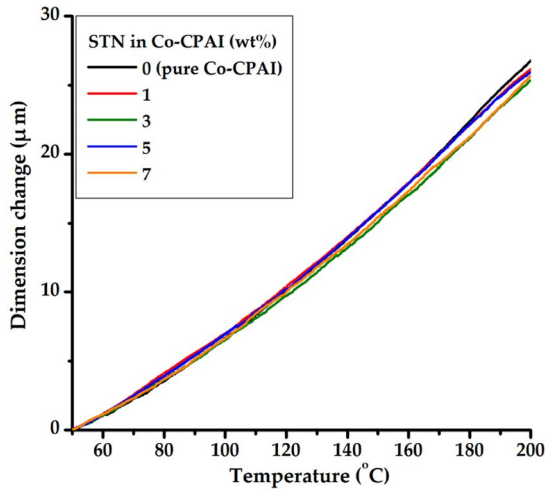

Fig. 8 TMA thermograms of Co-CPAI hybrids with various STN contents.

Table 2 Mechanical properties of Co-CPAI hybrid films

STN in Co-CPAI (wt%)	Ult. str.[a] (MPa)	Ini. mod.[b] (GPa)	E. B.[c] (%)
0 (pure Co-CPAI)	87	3.32	4
1	118	4.18	4
3	122	5.15	6
5	102	4.01	5
7	90	2.63	4

[a] Ultimate strength. [b] Initial modulus. [c] Elongation at break.

and orientation of the filler within the polymer matrix. The dramatic improvement in the mechanical properties of the films can be explained by the characteristics of the rigid plate-shaped clay dispersed in the nanoscale and the orientation of the dispersed clay in the matrix polymer.[53,54] However, when the STN content of the hybrid was increased from 3 to 7 wt%, the tensile strength and initial modulus of the films abruptly decreased to 90 MPa and 2.63 GPa, respectively (Table 2). These results are due to the fact that the excess clay forms aggregates above the critical content and acts as defects in the hybrid film,[55,56] as revealed by the XRD and TEM results (Fig. 4 and 5). Regardless of their STN content, however, all hybrid films showed a constant EB of 4–6% owing to the reinforcing effect provided by the clay. Fig. 9 shows the changes in the ultimate strength and initial modulus of Co-CPAI hybrid films with various STN content.

3.6 Optical transparency

The dispersed clay content and light transmittance of hybrid films are closely related. As the clay content in the matrix increases, the light transmittance of the hybrid film decreases because light cannot easily be transmitted in a film in which plate-shaped clay is evenly dispersed. The optical transparency of the hybrid films was evaluated by considering λ_o, which

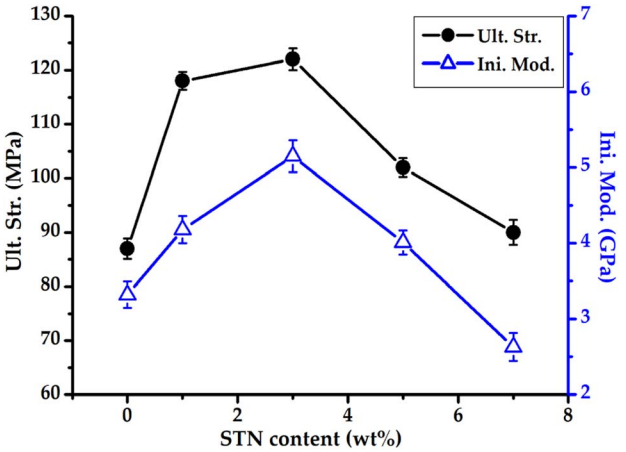

Fig. 9 Ultimate strength and initial modulus of Co-CPAI film.

represents the initial transmission wavelength, 500 nm^{trans} in the visible-light region, and YI.[57]

The UV-vis spectra of the hybrid films are shown in Fig. 10, and the corresponding absorption values are summarized in Table 3.

The λ_o values of the hybrid films were similar at 364–370 nm, regardless of their organoclay content. In addition, the 500 nm^{trans} values for all Co-CPAI hybrid films were very high (85–88%), regardless of their STN content. Clay is a multilayered mineral composed of several 1 nm-thick layers. In the hybrid films, as the clay increases beyond the critical content and agglomerates, light transmittance decreases. However, when the clay is exfoliated from the matrix at the nanometer scale, optically colorless and transparent films with very low YI values can be obtained. YI can be calculated using the following formula (ASTM E313-96, DIN 6167):

$$YI = 100 \times (aX - bZ)/Y,$$

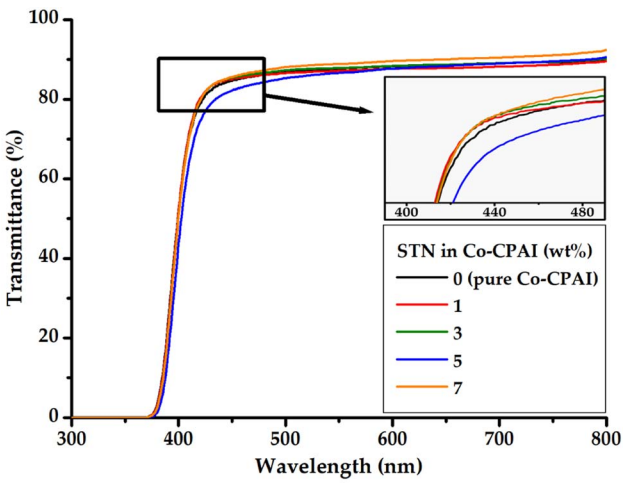

Fig. 10 UV-vis transmittances of Co-CPAI hybrid films with various STN contents.

© 2024 The Author(s). Published by the Royal Society of Chemistry

Open Access Article. Published on 18 March 2024. Downloaded on 6/4/2026 6:41:13 PM. This article is licensed under a Creative Commons Attribution-NonCommercial 3.0 Unported Licence.

Table 3 Optical transparencies of Co-CPAI hybrid films

STN in Co-CPAI (wt%)	Thickness[a] (μm)	λ_o[b] (nm)	500 nm^{trans} (%)	YI[c]
0 (pure Co-CPAI)	34	370	87	4
1	33	370	87	2
3	34	364	87	3
5	33	369	85	4
7	35	367	88	3

[a] Film thickness. [b] Cut-off wavelength. [c] Yellow index.

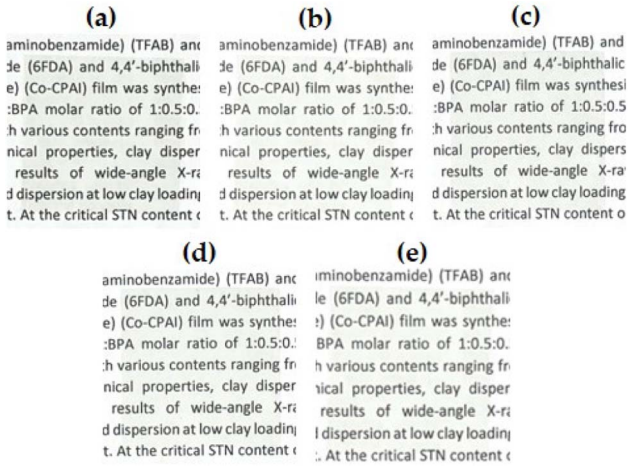

Fig. 11 Photographs of Co-CPAI hybrid films with various organoclay contents. (a) 0 (pure Co-CPAI), (b) 1, (c) 3, (d) 5, and (e) 7 wt% STN.

where a and b represent redness and yellowness, respectively, and X, Y, and Z represent tristimulus values.

Regardless of the organoclay content, the films revealed very low YI values of 2–4, which was consistent with the results obtained from λ_o and 500 nm^{trans}. Even the hybrid film prepared with over 7 wt% dispersed clay showed a YI of 3. These results indicate that the clay was evenly dispersed in the CPI matrix as nanosized particles that did not interfere with light transmission, as confirmed by the TEM results (Fig. 5). The Co-CPAI hybrid films synthesized in this study showed very low YI values because the entire polymer chain has an *m*-substituted monomer structure that prevents CTC formation by π-electrons and the clay in the matrix polymer is evenly distributed at the nanoscale level.

Fig. 11 displays images of hybrid films featuring various organoclay contents overlaid on a text, allowing for the examination of their optical transparency. The letter remains distinctly visible through the films, as all hybrid films maintain colorlessness and transparency, irrespective of their STN content.

4. Conclusions

Organoclays with surfaces that have been organically modified with alkyl groups can be used to prepare hybrid films with excellent physical properties that cannot be obtained through traditional compositing processes by utilizing the strong interaction between nanofillers and polymer matrices. Hybrid films with significantly improved physical properties can be obtained by dispersing a critical content of the filler into the polymer at the nanoscale level. These films demonstrate excellent potential as materials for electronic and optical applications.

In this study, a copolymer with a new monomer composition containing amide bonds was prepared, and Co-CPAI hybrid films containing 1–7 wt% organoclay (STN) were synthesized. The hybrid films were synthesized through step-by-step heat treatment after STN dispersion in the PAA state using the solution intercalation method. The thermomechanical properties, dispersed clay morphology, and optical transparency of hybrid films containing various STN contents were studied, and changes in their properties were compared. The hybrid films prepared with up to 3 wt% STN showed optimal physical properties, but these properties decreased above the critical content. Moreover, all hybrid films showed excellent optical transparency, regardless of their dispersed clay content. The excellent CTE and light transmittance of the hybrid films indicate their potential applications in the fields of flexible displays and electronic materials.

Conventional PI is widely used in films that require high-performance properties, but its dark brown color renders it difficult to apply as a display material. The new Co-CPAI hybrid films synthesized in this study using monomers with the appropriate structures may serve as suitable replacement materials for flexible-display and electronic materials that require both high thermomechanical properties and transparency.

Author contributions

J.-H. Chang designed the project and wrote the manuscript. L. K. Kwac and H. G. Kim reviewed and data analyzed. C. Na prepared the samples and participated in the data analysis. All authors have read and agreed to the published version of the manuscript.

Conflicts of interest

There are no conflicts to declare.

© 2024 The Author(s). Published by the Royal Society of Chemistry

Open Access Article. Published on 18 March 2024. Downloaded on 6/4/2026 6:41:13 PM. This article is licensed under a Creative Commons Attribution-NonCommercial 3.0 Unported Licence.

Acknowledgements

This research was supported by the Basic Science Research Program through the National Research Foundation of Korea (NRF) funded by the Ministry of Education (2016R1A6A1A03012069). This work also was supported by the National Research Foundation of Korea (NRF) grant funded the Korea Government (MSIT) (2022R1A2C1009863).

References

1 J. A. Rogers, T. Someya and Y. Huang, *Science*, 2010, **327**, 1603–1607.
2 M. Fahland, P. Karlsson and C. Charton, *Thin Solid Films*, 2001, **392**, 334–337.
3 M.-C. Choi, Y. Kim and C.-S. Ha, *Prog. Polym. Sci.*, 2008, **33**, 581–630.
4 D.-L. Liaw, K.-L. Wang, Y.-C. Huang, K.-R. Lee, J.-Y. Lai and C.-S. Ha, *Prog. Polym. Sci.*, 2012, **37**, 907–974.
5 K.-I. Fukukawa and M. Ueda, *Polym. J.*, 2008, **40**, 281–296.
6 C.-J. Chen, H.-J. Yen, Y.-C. Hu and G.-S. Liou, *J. Mater. Chem. C*, 2013, **1**, 7623–7634.
7 M. Nishihara, L. Christiani, A. Staykov and K. Sasaki, *J. Polym. Sci., Part B: Polym. Phys.*, 2014, **52**, 293–298.
8 T. Omote, T. Yamaoka and K. Koseki, *J. Appl. Polym. Sci.*, 1989, **38**, 389–402.
9 J. W. Xu, M. L. Chng, T. S. Chung, C. B. He and R. Wang, *Polymer*, 2003, **44**, 4715–4721.
10 M. Hasegawa, Y. Hoshino, N. Katsura and J. Ishii, *Polymer*, 2017, **111**, 91–102.
11 Y. Zhuang, J. G. Seong and Y. M. Lee, *Prog. Polym. Sci.*, 2019, **92**, 35–88.
12 A. Y. Kim, S. J. Lee, M. Y. Choi, C. Na, L. K. Kwac, H. G. Kim and J.-H. Chang, *RSC Adv.*, 2023, **13**, 24423–24431.
13 I. H. Choi, B. Sohn and J.-H. Chang, *Appl. Clay Sci.*, 2010, **48**, 117–126.
14 T.-L. Li and S. L.-C. Hsu, *Thin Solid Films*, 2010, **518**, 6761–6766.
15 J. Ju and J.-H. Chang, *Macromol. Res.*, 2014, **22**, 549–556.
16 R. Yokota, S. Yamamoto, S. Yano, T. Sawaguchi, M. Hasegawa, H. Yamaguchi, H. Ozawa and R. Sato, *High Perform. Polym.*, 2001, **13**, S61–S72.
17 J.-E. Han, B.-K. Jeon, B.-J. Goo, S. H. Cho, S.-H. Kim, K.-S. Lee, Y.-H. Park and J.-Y. Lee, *Polymer*, 2009, **33**, 91–95.
18 Y.-Y. Liu, J.-H. Cao, Y. Wang, S.-G. Shen, W.-H. Liang and D.-Y. Wu, *ACS Appl. Polym. Mater.*, 2022, **4**, 7664–7673.
19 S. K. Lim, L. Setiawan, T.-H. Bae and R. Wang, *J. Membr. Sci.*, 2016, **501**, 152–160.
20 A. Sarkar, P. N. Honkhambe, C. V. Avadhani and P. P. Wadgaonkar, *Eur. Polym. J.*, 2007, **43**, 3646–3654.
21 M. Bhattacharya, *Materials*, 2016, **9**, 262–296.
22 N. Bitinis, M. Hernandez, R. Verdejo, J. M. Kenny and M. A. Lopez-Manchado, *Adv. Mater.*, 2011, **23**, 5229–5236.
23 J. Zhang, C. H. Zhou, S. Petit and H. Zhang, *Appl. Clay Sci.*, 2019, **177**, 114–138.
24 J. M. García-Martínez, O. Laguna, S. Areso and E. P. Collar, *J. Polym. Sci., Part B: Polym. Phys.*, 2000, **38**, 1564–1574.
25 W. F. Jaynes and J. M. Bigham, *Clays Clay Miner.*, 1987, **35**, 440–448.
26 H.-S. Jin and J.-H. Chang, *Polymer*, 2008, **32**, 256–262.
27 C.-Y. Yang, S. L.-C. Hsu and J. S. Chen, *J. Appl. Polym. Sci.*, 2005, **98**, 2064–2069.
28 T. Nakano, S. Nagaoka and H. Kawakami, *Polym. Adv. Technol.*, 2005, **16**, 753–757.
29 M. Niwa, S. Nagaoka and H. Kawakami, *J. Appl. Polym. Sci.*, 2006, **100**, 2436–2442.
30 M. Y. Choi, S. J. Lee, L. K. Kwac, H. G. Kim and J.-H. Chang, *RSC Adv.*, 2021, **11**, 30479–30486.
31 Y. D. Lee, K. Kim, Y. Ok, M. Kim and J.-H. Chang, *Polymer(Korea)*, 2016, **40**, 298–305.
32 K. Kawasaki, T. Ebina, F. Mizukami, H. Tsuda and K. Motegi, *Appl. Clay Sci.*, 2010, **48**, 111–116.
33 W. Wong-Ng, H. F. McMurdie, C. R. Hubbard and A. D. Mighell, *J. Res. Natl. Inst. Stand. Technol.*, 2001, **106**, 1013–1028.
34 A. Phuruangrata, T. Thongtemb and S. Thongtem, *J. Exp. Nanosci.*, 2010, **5**, 263–270.
35 D. L. Pavia, G. M. Lampman, G. S. Kriz and J. A. Vyvyan, *Introduction to Spectroscopy*, Cengage Learning, Boston, Massachusetts, USA, 2008, ch. 2, pp. 14–95.
36 D. L. Pavia, G. M. Lampman, G. S. Kriz and J. A. Vyvyan, *Introduction to Spectroscopy*, Cengage Learning, Boston, Massachusetts, USA, 2008, ch. 4, pp. 146–183.
37 R. A. Vaia and E. P. Giannelis, *Macromolecules*, 1997, **30**, 8000–8009.
38 D. Porter, E. Metcalfe and M. J. K. Thomas, *Fire Mater.*, 2000, **24**, 45–52.
39 K. Yano, A. Usuki, A. Okada, T. Kurauchi and O. Kamigaito, *J. Polym. Sci., Part A: Polym. Chem.*, 1993, **31**, 2493–2498.
40 I. H. Choi and J.-H. Chang, *Polym. Adv. Technol.*, 2011, **22**, 682–689.
41 A. B. Morgan and J. W. Gilman, *J. Appl. Polym. Sci.*, 2003, **87**, 1329–1338.
42 J. Ma, J. Xu, J.-H. Ren, Z.-Z. Yu and Y.-W. Mai, *Polymer*, 2003, **44**, 4619–4624.
43 S. W. Kim and H. M. Choi, *High Perform. Polym.*, 2014, **27**, 694–704.
44 T. Agag and T. Takeichi, *Polymer*, 2000, **41**, 7083–7090.
45 H. A. Khonakdar, S. H. Jafari and R. Hässler, *J. Appl. Polym. Sci.*, 2007, **104**, 1654–1660.
46 C.-H. Choi, Y.-M. Kim and J.-H. Chang, *Polym. Sci. Technol.*, 2012, **23**, 296–306.
47 S. J. Lee, M. Y. Choi, L. K. Kwac, H. G. Kim and J.-H. Chang, *Polymers*, 2022, **14**, 2469.
48 O. Becker, R. J. Varley and G. P. Simon, *Eur. Polym. J.*, 2004, **40**, 187–195.
49 J. Zhu, F. M. Uhl, A. B. Morgan and C. A. Wilkie, *Chem. Mater.*, 2001, **13**, 4649–4654.
50 A. H. Farha, A. F. Al Naim and S. A. Mansour, *Polymers*, 2020, **12**, 1935.
51 S. L.-C. Hsu, U. Wang, J.-S. King and J.-L. Jeng, *Polymer*, 2003, **44**, 5533–5540.
52 F. Liu, Z. Liu, S. Gao, Q. You, L. Zou, J. Chen, J. Liu and X. Liu, *RSC Adv.*, 2018, **8**, 19034–19040.

© 2024 The Author(s). Published by the Royal Society of Chemistry

Open Access Article. Published on 18 March 2024. Downloaded on 6/4/2026 6:41:13 PM.
This article is licensed under a Creative Commons Attribution-NonCommercial 3.0 Unported Licence.

53 W. J. Bae, M. K. Kovalev, F. Kalinina, M. Kim and C. Cho, *Polymer*, 2016, **105**, 124–132.
54 T. Agag, T. Koga and T. Takeichi, *Polymer*, 2001, **42**, 3399–3408.
55 S. Sequeira, D. V. Evtuguin and I. Portugal, *Polym. Compos.*, 2009, **30**, 1275–1282.
56 M.-D. Damaceanu, C.-P. Constantin, A. Nicolescu, M. Bruma, N. Belomoina and R. S. Begunov, *Eur. Polym. J.*, 2014, **50**, 200–213.
57 S. Srivastava, M. Haridas and J. K. Basu, *Bull. Mater. Sci.*, 2008, **31**, 213–217.

© 2024 The Author(s). Published by the Royal Society of Chemistry